Assessing Dolomite Surface Reactivity at Temperatures from 40 to 120 °C by Hydrothermal Atomic Force Microscopy

Ulf-Niklas Berninger[1,2]*, Giuseppe D. Saldi[1], Guntram Jordan[2], Jacques Schott[1], Eric H. Oelkers[1,3]

[1] *Géoscience Environnement Toulouse, CNRS-UPS-OMP, 14 av. Édouard Belin, 31400 Toulouse, France.*

[2] *Dept. für Geo- und Umweltwissenschaften, Ludwig-Maximilians-Universität München, Theresienstr. 41, 80333 München, Germany.*

[3] *Department of Earth Sciences, UCL, Gower Street, WC1E 6BT London, United Kingdom.*

* *Corresponding author e-mail:* berninger@get.obs-mip.fr

Abstract - This study investigated the reactivity of the (104) dolomite surface in the system $MgCO_3$-$CaCO_3$-NaCl-H_2O via a suite of aqueous solution-dolomite hydrothermal atomic force microscopy interaction experiments at temperatures from 40 to 120 °C, pH ranging from 4 to 8, pressures up to 5 bars, and over a wide range of aqueous fluid saturation state. Dolomite dissolution was observed in the presence of undersaturated aqueous fluids. Dissolution produced crystallographically well defined etch pits, consistent with the stoichiometric release of ordered lattice cations. In low to moderately saturated fluids, dolomite growth began by the growth of one or two layers of carbonate (layer height < 3 Å) which morphologically reproduced the initial surface features, resembling the template effect as previously described by Astilleros *et al.* (2003, 2006) and Freij *et al.* (2004). Further growth was strongly inhibited and did not show any systematic crystallographically oriented growth morphologies. At aqueous fluid saturation states exceeding 500, nucleation and growth was observed on the dolomite surfaces at moderate rates, but these did not exhibit the characteristic dolomite crystallographic orientation after the growth of several layers. Taken

together these observations suggest that the direct precipitation of dolomite from aqueous solution is unflavored at temperatures to at least 120 °C due to the poisioning of the dolomite surface for further growth by the precipitation one to four Ca-Mg carbonate layers on these surfaces.

1 Introduction

Dolomite [$CaMg(CO_3)_2$] is the second most abundant carbonate mineral in the Earth's crust (*e.g.*, Warren, 2000). Knowledge of dolomite precipitation and dissolution rates is essential for modeling major natural and industrial processes including the formation of sedimentary carbonates (Baker and Kastner, 1981), carbon capture and storage (Xu *et al.*, 2003; Moore *et al.*, 2005; Oelkers *et al.*, 2008; Wang *et al.*, 2013; Tutolo *et al.*, 2014), the preservation of paleoenvironmental signatures in carbonate rocks (Fantle and DePaolo, 2007; Fantle and Higgins, 2014; Fantle, 2015), secondary oil recovery (Wang *et al.*, 2013), and ocean chemistry (Mackenzie and Morse, 1992; Mackenzie and Andersson, 2013).

The formation of dolomite in natural and laboratory systems is, however, confounding (Arvidson and Mackenzie, 1999). Seawater is strongly supersaturated with respect to dolomite but there is no evidence of abiotic dolomite precipitation in modern marine depositional environments; in contrast, the ancient sedimentary record often contains dolomite (Tribble *et al.*, 1995; Hardie, 1996; Berner and Berner, 1996; Stanley and Hardie, 1999; Lowenstein *et al.*, 2001; Berner, 2004; Holland, 2005). Abiotic laboratory synthesis of dolomite generally requires hydrothermal conditions (Graf and Goldschmidt, 1956; Katz and Matthews, 1977; Kessels *et al.*, 2000). The lack of abiotic low temperature ($< 100 \ °C$) dolomite formation has been interpreted as a kinetic limitation potentially due to the slow dehydration rates of the aqueous Mg^{2+} cation (Lippmann, 1973; Higgins and Hu, 2005; Saldi

et al., 2009, 2012; Berninger *et al.* 2014, 2016).Alternatively, Roberts et al. (2013) reported the nucleation of ordered dolomite nanocrystals at 30 °C in association with high density carboxylated surfaces, and sugested that the presence of Mg bound carboxylic groups can reduce the energy required for carbonation and attachement of Ca^{2+}.

Numerous laboratory studies suggested that microorganisms facilitate the formation of dolomite at low temperatures. Microbes that have been implicated in low temperature dolomite formation include sulfate-reducing bacteria (Vasconcelos *et al.*, 1995; Vasconcelos and McKenzie, 1997; Warthmann *et al.*, 2000; van Lith *et al.*, 2003; Wright and Wacey, 2005), sulfide oxidizers (Moreira *et al.*, 2004), and moderately halophilic aerobic heterotrophs (Sánchez-Román *et al.*, 2008). Many of these studies observe disordered or iron-rich dolomite forming on cell surfaces, raising the possibility that dolomite nucleation is surface-mediated rather than driven by metabolic processes.

This study was initiated to further illuminate the processes and mechanisms responsible for the inhibition of abiotic dolomite precipitation at ambient conditions. Towards this goal the dissolution or growth of dolomite from aqueous solution was monitored on its surface using hydrothermal atomic force microscopy (HAFM) at temperatures from 40 to 120 °C. This temperature range was chosen for two reasons. First, dolomite is reported to precipitate from aqueous solutions at temperatures in excess of 140 °C (Rodriguez-Blanco *et al.*, 2015). Second, recent work on the anhydrous carbonate mineral magnesite shows that this mineral precipitates sufficiently fast at 80 to 120 °C to be measured directly using HAFM (Saldi *et al.*, 2009, 2012; Gautier *et al.*, 2015; Berninger *et al.*, 2016). This latter observation suggests that this method may also be applicable to quantify dolomite growth at these conditions. The purpose of this manuscript is to present the results of this HAFM study of dolomite growth and to use these results to improve our understanding of dolomite reactivity in natural systems.

2 Materials, chemical analysis, and experimental methods

2.1 Geochemical calculations

The standard state adopted in this study is that of unit activity for pure minerals and H_2O at any temperature and pressure. For aqueous species other than H_2O, the standard state is unit activity of the species in a hypothetical 1 molal solution referenced to infinite dilution at any temperature and pressure. Dolomite precipitation or dissolution can be described using

$$CaMg(CO_3)_2 = Ca^{2+} + Mg^{2+} + 2CO_3^{2-} \tag{1}$$

In accord with the standard state, the law of mass action for reaction (1) can be written

$$K_{sp(Dol)} = a_{eq,Ca^{2+}} a_{eq,Mg^{2+}} a^2_{eq,CO_3^{2-}} \tag{2}$$

where $a_{eq,i}$ refers to the activity of the subscripted aqueous species at equilibrium and $K_{sp(Dol)}$ designates the equilibrium constant for reaction (1). The saturation state of the aqueous fluid with respect to dolomite, Ω_{Dol}, can then be written

$$\Omega_{Dol} = \frac{a_{Ca^{2+}} a_{Mg^{2+}} a^2_{CO_3^{2-}}}{K_{sp(Dol)}} \tag{3}$$

where a_i refers to the activity of the subscripted aqueous species. All thermodynamic calculations reported in the present study were performed using PHREEQC (Parkhurst and Appelo, 1999). Aqueous activity coefficients in this model were generated using the 'b-dot' activity model (Helgeson, 1969). The thermodynamic database used in these calcualtions was a slightly modified version of the llnl database. Much of data present in the llnl database of PHREEQC originates from SUPCRT92 (Johnson *et al.*, 1992). The llnl database was modified to include the equilibrium constants for Mg^{2+} hydrolysis and the carbonic acid dissociation reported by Brown *et al.* (1996) and Millero *et al.* (2007), respectively.

2.2 Hydrothermal atomic force microscopy (HAFM) experiments

Hydrothermal atomic force microscopy dolomite growth experiments were performed using in-house constructed continuous-flow HAFM operating in contact mode fitted with uncoated silicon cantilevers purchased from Nanosensors. The system allows for *in-situ* visualization of relatively flat mineral surfaces at temperatures up to 150 °C and pressures up to 50 bars (*cf.*, Higgins *et al.*, 1998; Jordan et al., 1999; Aldushin *et al.*, 2004; Jordan and Astilleros, 2006). The experiments in this study were performed at temperatures up to 120 °C with confining pressures of no more than 5 bars. Experiments were not performed at higher temperature because preliminary tests showed that it was not possible to obtain high quality images at such conditions due primarily to the rapid degradation of the cantilever tip in contact with the reactive aqueous solution compositions. Each experiment lasted from 2 to 7 hours total. Experiments were performed by passing a reactive fluid over a cleaved dolomite grain orientated to expose its (104) surface. Inlet fluids were placed in either Viton containers above the HAFM cell allowing gravitational fluid feed or a flexible pressurized container promoting flow through the HAFM cell. Fluid flow rates were approximately 10 μg/s allowing the rapid renewal of the fluid within the ~500 μL reaction cell. Due to the rapid fluid renewal and a mineral surface area of only a few mm^2, the chemical composition of the inlet fluid was negligibly affected by fluid-mineral reactions occurring in the reaction cell.

Experiments were performed on natural transparent dolomite single crystals from 1) Eugui, Spain (purchased from Fabre Minerals) and 2) Sunk, Austria (obtained from the Museum Reich der Kristalle in Munich, Germany). The composition of these dolomites were determined using a Cameca SX 100 electron microprobe; the results of these analyses are provided in Table 1. These dolomites contain slightly more calcium than magnesium due to

the presence of ~ 2 % Fe, which is most likely located in the magnesium site. The mineralogy of these solids were determined using an INEL CPS-120 diffractometer with Co K_α-radiation, $\lambda = 1.78897$ Å, and a graphite monochromator. X-ray diffraction was performed from 1 to 110º 2θ at 0.09º/min and at a step size of 0.029º. These diffractograms, provided in the electronic supplement, show the initial solids to be pure dolomite. They also show strong superstructure reflections (*e.g.*, Lippmann, 1973) indicating that these dolomites are highly ordered. The crystals were cleaved with a scalpel immediately before being fixed in the HAFM cell orienting the (104) surface perpendicular to the tip of the cantilever. The (104) dolomite cleavage surface was chosen for this growth study 1) due to ease of preparation, and 2) because this surface contains equal amounts of calcium and magnesium. The HAFM flow system was then pressurized and the cell heated to the desired temperature at the start of each experiment.

2.3 Reactive fluids and their analysis

The inlet fluids of all experiments consisted of high purity deionized water (resistivity 18.2 MΩ cm), and reagent grade NaCl, 1N HCl, $NaHCO_3$, $MgCl_2 \cdot 6H_2O$, and $CaCl_2 \cdot 2H_2O$ as well as dry ice purchased from Linde. The inlet fluid compositions for all experiments are summarized in Table 2.

Aqueous magnesium and calcium concentrations were measured by flame atomic absorption spectroscopy using a Perkin Elmer AAnalyst 400 Atomic Absorption Spectrometer with an uncertainty of $\pm$ 2 % and detection limits of 1 x 10^{-7} and 2 x 10^{-7} mol/kg, respectively. Alkalinity was determined by standard HCl titration using Schott TA 10plus with an uncertainty of $\pm$ 1 % and a detection limit of 2 x 10^{-5} eq/L. Reactive fluid pH measurements were performed at room temperature immediately before and after the performed experiments using a standard glass electrode, previously calibrated with 4.01, 6.86, and 9.18 NIST pH

buffers. The uncertainty of these measurements is estimated to be ± 0.05 pH units. Fluid pH, speciation, and saturation state with respect to dolomite at the temperature of each experiment were calculated by PHREEQC (Parkhurst and Appelo, 1999) using pH values and fluid compositions measured at 25 °C.

3 Results

In total of 71 HAFM experiments were performed in this study at temperatures ranging from 40 to 100 °C. Eleven of these experiments were performed using Eugui dolomite and 60 using Sunk dolomite. A summary of the experimental conditions, measured reactive fluid chemistry, the saturation state of the fluid phase with respect to dolomite, and observed dolomite growth behavior is presented in Table 3. Several distinct behaviors were observed as described below.

In 15 experiments, the reactive fluid was undersaturated with respect to dolomite as indicated by a saturation state of < 1 in *Table 3*. Dolomite dissolution was also observed in experiment Sunk-23; the reactive fluid in this experiment was calculated to be slightly super-saturated with respect to dolomite. This ambiguity may be due to the uncertainties in the thermodynamic database at the conditions of this 40 °C experiment. A representative example of observed dolomite dissolution behavior at 100 °C is shown in Figure 1. Well defined etch pits that follow the crystallographic directions $[\bar{4}41]$ and $[48\bar{1}]$ of the dolomite substrate are observed to form. Dolomite step retreat velocities in this experiment were too rapid to obtain unambiguous retreat rates. Another example of etch-pits forming during the dissolution of dolomite cleavage surface is provided in Fig. 2, where dolomite was dissolved at 80 °C under more basic conditions (pH = 8.14). Because of its lower symmetry, the observed etch pits exhibit a shape that deviates from the rhombic form typically observed in calcite group minerals (cf. Higgins and Hu, 2005; Xu et al., 2013). The relatively slow dissolution rates

observed at these conditions allowed determination of the the corresponding etch pit spreading rates: the steps moved apart from each other at the distinct rates of 0.81 ±0.21 nm/s and 0.66 ±0.28 nm/s, for the obtuse and acute $[\bar{4}41]$ and $[48\bar{1}]$ steps, respectively.

In 10 experiments no dolomite dissolution or precipitation was observed. The reactive fluid saturation state in these experiments ranged from 2.8 to 13.6, other than one experiment with a saturation index of 28.1 (experiment Sunk-18). This latter experiment was that having the lowest reactive fluid divalent cation concentrations; aqueous Ca^{2+} and Mg^{2+} activities were calculated to be ~ 9×10^{-7} and ~ 1×10^{-6}, respectively, in this experiment. The relatively high degree of saturation state of this experiment is due to the high reactive fluid alkalinity and comparatively high pH. A representative example of an unreacting dolomite surface during a representative experiment is shown in Fig. 3.

In 33 experiments a single dolomite growth layer was observed to form. The saturation states of the reactive fluids with respect to dolomite in these experiments ranged from 7.3 to 336. The height of the observed growth layers is observed to be < 3.0 Å, consistent with the formation of a monolayer of carbonate. A representative example of such observations is shown in Fig. 4. It can be seen in this figure that the first layer grows via step advancement to the point at which a full monolayer is completed after which growth is significantly inhibited. The first growth layer was typically complete within the first hour of each experiment; a second layer was not observed despite allowing the experiment to continue for an additional 2 to 6 hours. Thus, the step morphology of the starting surface is reproduced once the first layer is complete, similar to the results observed by Higgins and Hu (2005) for dolomite growth at 27 °C.

In 13 experiments multiple layers of dolomite growth was observed. The saturation states of the reactive fluids with respect to dolomite in these experiments ranged from 16.6 to 1514.

8

A representative example of these observations can be seen in Fig. 5. The growth of the first layer in these experiments is similar to that of the experiments exhibiting the growth of only a single layer. After this first layer forms, subsequent layers grow at a slower rate. For instance, during the experiment Eugui-10 (Fig. 5), the measured etch pit closing rate due to growth decreased by 30 %, changing in one direction from 1.04 to 0.70 nm/s, when the second layer started to grow. It was also observed that, whereas the first growth layer follows the morphology of the dolomite substrate, the subsequent growth layers form more rounded 'growth island morphologies', each subsequent layer following less the original morphological form of the starting dolomite substrate. In each case the growth of dolomite continued through the end of the experiment.

The formation of 2 or more layers was observed for Ω_{Dol} as low as 16 at 100 °C, whereas it was necessary to increase significantly the degree of supersaturation of the reacting fluids to provoke the formation of a second layer at lower temperatures. An increase of the saturation ratio to above 300 was insufficient to promote the formation of multiple layers at 60 °C (e.g. Eugui-03-B) but, as shown in Fig. 5, a relatively rapid formation of three consecutive layers was observed at 80 °C for $\Omega_{Dol} = 478$. The growth of multiple layers was appreciably accelerated at 90 and 100 °C in the presence of fluids with $\Omega_{Dol} > 650$ (Fig. 6 and 7). At these conditions, however, the step growth mechanism became very chaotic: the rates of advancement of the steps parallel to $[\bar{4}41]$ and $[48\bar{1}]$ was outpaced by the irregular growth of layers displaying a faster reaction front along a direction sub-parallel to the steps originated by dissolution. In particular, this irregular growth mode (Fig. 7) hampered the development of the typical straight morphology of [441] acute steps by the formation of elongated lozenge-shaped layers following the [481] direction. The growth of these layers was coupled to the formation of non-oriented two-dimensional nuclei, which occurred during the experiments conducted at 90 and 100 °C (experiments Eugui-11A and 11B, Fig.6) with the highest values

9

of fluid supersaturation (Ω_{Dol} = 933 and 1514, respectively).

4 Discussion

4.1 Comparison with past results

A number of past studies have attempted to precipitate dolomite abiotically at temperatures less than 200 °C. Most, and perhaps all of these past attempts failed to precipitate stoichiometric, well crystallized dolomite. For example, Land (1998) failed to precipitate dolomite from supersaturated aqueous solutions at 25 °C despite a 32-year long experiment. Higgins and Hu (2005) and Hu *et al.* (2005) attempted to precipitate dolomite at 27 °C by monitoring the reaction progress using atomic force microscopy on the (104) dolomite surface. As was observed in the present study, a single layer of dolomite was rapidly formed on the existing dolomite surface but additional layers were strongly inhibited from growing. Arvidson and Mackenzie (1999) attempted to measure the precipitation rates of dolomite at temperatures of 100 to 200 °C in mixed-flow reactors but rather succeeded in measuring the steady-state precipitation rates of a calcium-rich protodolomite on the surface of dolomite seeds. These authors provided a rate equation to describe their protodolomite precipitation rates as a function of temperature and saturation state. Our results are largely consistent with these past observations, as we observed the precipitation of a single dolomite layer on the original dolomite surface followed by a far slower growth of a poorly defined Mg-Ca-carbonate. As suggested by Higgins and Hu (2005) and later confirmed by the observations of Fenter et al. (2007), the formation of a self-limited layer on dolomite surface can be attributed to the lattice strain associated with the different composition of a Ca-rich overgrown layer and the dolomite substrate. These authors also observed that the composition of the growth layers is sensitive to the Mg/Ca ratio of the reactive aqueous solution (see next section) and

suggested that an appropriate solution composition might lead to the growth of an unstrained 1:1 Mg/Ca ratio layer. However, the need to order Ca and Mg into the dolomite structure makes the formation of stoichiometric and ordered epitaxial layers unlikely at room temperature, because of the slow H_2O exchange rates in the hydration shell of Mg ions. The results of the present study indicate that neither increasing temperature nor high Mg^2/Ca^{2+} activity ratios promote the direct formation of dolomite monolayers, as the growth of disordered/hydrated protodolomite-type layers are kinetically favored at the conditions considered in this study. In contrast, Rodriguez-Blanco *et al.* (2015) argued that they crystallized dolomite from aqueous solutions at temperatures from 60 to 220 °C via a mechanism that transforms an originally precipitated amorphous calcium carbonate into crystalline stoichiometric dolomite via a protodolomite precursor. Only at temperatures > 140 ℃ they did no longer observe the formation of protodolomite as an intermediate step. It should be emphasized however that the evidence presented by these authors for the presence of an ordered dolomite in their experiments is based on the observations of superstructural reflections that may not have been significant considering their signal intensity compared with that of the background signal, indicating a very low degree of ordering. It should also be noted that although numerous studies have argued that dolomite is readily formed biotically (*e.g.*, Warthman *et al.*, 2000), such conclusions have been questioned by Gregg *et al.* (2015) who reexamined published X-ray diffraction data, concluding that dolomite synthesis in the laboratory under near-ambient conditions by microbial mediation are unsubstantiated.

4.2 What inhibits dolomite precipitation at temperatures ≤ 120 ℃?

The results described above show that a single layer of carbonate is readily precipitated on the surface of dolomite. This first layer closely mimics the surface of the original dolomite consistent with epitaxial growth. Subsequent layers, however, are more sluggish to form and do not follow the original surface structure. These subsequent layers tend also to form as

distinct growth islands on the surface of the first epitaxial growth layer if sufficient temperature and solution supersaturation are present in the system. As mentioned above, such observations are consistent with the results reported by Higgins and Hu (2005). These authors suggested that this behavior stemmed from the likelihood that the first layer precipitated on the dolomite surface was non-stoichiometric and non-ordered due to the high affinity of calcium compared to magnesium for the dolomite surface. This non-stoichiometric, non-ordered layer then serves as a poor template for further growth because of its increased surface free energy. Lateral force frictional data obtained across the boundaries between the first grown layer and the dolomite substrate supports this conclusion, showing a Ca-enrichment of the overgrowth. X-ray photoelectron spectroscopy (XPS) analyses of the dolomite surface exposed to supersaturated solutions having equal Ca^{2+} and Mg^{2+} activities (Hu et al., 2006) as well as X-ray reflectivity data (Fenter et al., 2007) also evidences the formation of a disordered Ca-rich self-limiting layer with a Ca/Mg ratio varying between 2 and 6. Nevertheless, a recent XPS study of the products of dolomite growth experiments described by Berninger (2016), performed in bulk chemical reactors at 150-175 °C, show that the composition of the precipitated surface layers is mildly enriched in magnesium at the outermost surface. In addition, scanning electron microscope analysis of the grains collected from the Berninger (2016) experiments shows the development of distinct growth islands on the surface of the original seed crystals. These observations seem to be in agreement with our results. At the temperatures and aqueous Mg/Ca ratios considered in this study (see Tables 2 and 3), the formation of growth layers somewhat enriched in Mg should be favored. The observed more rapid layer growth velocities in the direction of the acute steps movement (Fig. 6) is also in agreement with this hypothesis, since Mg was observed to be preferentially adsorbed at the acute steps terminations of calcite and Mg-calcite (Paquette and Reeder, 1995; Davis et al., 2000).

Taken together, these observations suggest that dolomite growth starting from ambient temperature up to 120 ℃ is self-inhibited by the initial precipitation of a non-stoichiometric disordered Mg-Ca-carbonate which then disfavors the further epitaxial growth on this surface. Subsequent growth requires nucleation at new growth sites on the substrate. This is supported by the relatively slow formation of growth islands, which likely occur at defects generated during the growth the first layer (cf. Higgins and Hu, 2005). Due to the lack of surface templating, these growth islands are likely poorly ordered and non-stoichiometric, consistent with our observations.

4.3 Consequences for mineral carbonation

The possibility of storing carbon in the subsurface as dolomite is particularly attractive as it is highly stable and its formation can take advantage of large quantities of magnesium present in basalts and ultramafic rocks (*cf.*, Oelkers *et al.*, 2008; Kaszuba *et al.*, 2011; Gislason and Oelkers, 2014; Matter *et al.,* 2016). Moreover a number of geochemical modeling studies have suggested that dolomite is thermodynamically favored to precipitate during the injection of CO_2 into the subsurface as part of carbon capture and storage efforts (*e.g.*, Xu *et al.*, 2003; Gysi and Stefánsson, 2008). The results of this study illustrate that the precipitation of dolomite via abiotic processes is sluggish and/or not possible at temperatures up to 120 ℃. As such it seems unlikely that dolomite would be an effective mineralogical carbon storage host in *in-situ* mineral carbonation systems at least at temperatures < 120 °C. It should be noted, however, that the results of Gysi and Stefánsson (2012) suggest that dolomite-ankerite solid solutions might readily form at these conditions providing the means to carbonate magnesium during subsurface carbon storage efforts.

5 Conclusion

The results summarized above provide further insight into the inhibition of abiotic dolomite growth in low temperature systems. Most notably these results support the hypothesis that the first dolomite growth layer formed on dolomite substrate poisons this surface, inhibiting further growth. The results show that this behavior is not just limited to ambient temperature, but well extends to the mildly hydrothermal temperatures. Additional growth appears to require surface nucleation and results in the formation of a somewhat non-stoichiometric and/or poorly ordered dolomite-like phase. As such it seems that the most likely route for the formation of dolomite in natural systems may be via the recrystallization of a poorly crystalline and/or non-stoichiometric and disordered protodolomite such as suggested by Kaczmarek and Sibley (2007, 2014) and Montes-Hernandez *et al.* (2014).

REFERENCES

Aldushin K., Jordan G., Rammensee W., Schmahl W.W. and Becker H.-W. (2004) Apophyllite (001) surface alteration in aqueous solutions studied by HAFM. *Geochimica et Cosmochimica Acta*, **68**, 217-226.

Arvidson R.S. and Mackenzie F.T. (1999) The dolomite problem: Control of precipitation kinetics by temperature and saturation state. *American Journal of Science*, **299**, 257-288.

Astilleros J.M., Pina C.M., Fernández-Díaz L., Prieto M. and Putnis A. (2006) Nanoscale phenomena during the growth of solid solutions on calcite $\{10\bar{1}4\}$ surfaces. *Chemical Geology*, **225**, 322-335.

Astilleros J.M., Pina C.M., Fernández-Díaz L. and Putnis A. (2003) Metastable phenomena on calcite $\{10\bar{1}4\}$ surfaces growing from Sr^{2+}-Ca^{2+}-CO_3^{2-} aqueous solutions. *Chemical Geology*, **193**, 93-107.

Baker P.A. and Kastner M. (1981) Constraints on the formation of sedimentary dolomite. *Science*, **213**, 214-216.

Berner E.K. and Berner R.A. (1996) *Global environment: Water, air, and geochemical cycles*. Prentice Hall, Englewood Clifts, New Jersey. 376 pp.

Berner R.A. (2004) A model for calcium, magnesium and sulfate in seawater over Phanerozoic time. *American Journal of Science*, **304**, 438-453.

Berninger U.-N. (2016) The reactivity of Mg-bearing carbonate minerals. Ph.D. thesis Université Paul Sabatier, Toulouse. France, 243 p.

Berninger U.-N., Jordan G., Lindner M., Reul A., Schott J. and Oelkers E.H. (2016) On the effect of aqueous Ca on magnesite growth – Insight into trace element inhibition of carbonate mineral growth. *Geochimica et Cosmochimica Acta*, **178**, 195-209.

Berninger U.-N., Jordan G., Schott J. and Oelkers E.H. (2014) The experimental determination of hydromagnesite precipitation rates at 22.5 to 75 °C. *Mineralogical Magazine*, **78**, 1405-1416.

Brown P.L., Drummond S.E. and Palmer D.A. (1996) Hydrolysis of magnesium (II) at elevated temperatures. *Journal of the Chemical Society-Dalton Transactions,* **1996**, 3071-3075.

Davis K.J., Dove P.M., and De Yoreo J.J. (2000) The role of Mg^{2+} as an impurity in calcite growth. *Science* **290**, 1134-1137.

Fantle M.S. (2015) Calcium isotopic evidence for rapid recrystallization of bulk marine carbonated and implications for geochemical proxies. *Geochimica et Cosmochimica Acta*, **148**, 378-401.

Fantle M.S. and DePaolo D.J. (2007) Ca isotopes in carbonate sediment and pore fluid from ODP Site 807A: The Ca^{2+}(aq)-calcite equilibrium fractionation factor and calcite recrystallization rates in Pleistocene sediments. *Geochimica et Cosmochimica Acta*, **71**, 2524-2546.

Fantle M.S. and Higgins J. (2014) The effects of diagenesis and dolomitization on Ca and Mg isotopes in platform carbonates: Implications for the geochemical cycles of Ca and Mg. *Geochimica et Cosmochimica Acta*, **142**, 458-481.

Fenter, P., Zhang, Z., Park, C., Sturchio, N., F, X., & Higgins, S. (2007). Structure and reactivity of the dolomite (104)-water interface: New insights into the dolomite problem. *Geochim. Cosmochim. Acta*, **71**, 566-579.

Freij S.J., Putnis A. and Astilleros J.M. (2004) Nanoscale observations of the effect of cobalt on calcite growth and dissolution. *Journal of Crystal Growth*, **267**, 288-300.

Gautier Q., Berninger U.-N., Schott J. and Jordan G. (2015) Influence of organic ligands on magnesite growth: A hydrothermal atomic force microscopy study. *Geochimica et Cosmochimica Acta*, **155**, 68-85.

Gislason, S.R. and Oelkers, E.H. (2014) Carbon storage in basalt. *Science,* **344,** 373-374.

Graf D.L. and Goldsmith J.R. (1956) Some hydrothermal syntheses of dolomite and protodolomite. *Journal of Geology*, **64**, 173-186.

Gregg J.M., Bish D.L., Kaczmarek S.E. and Machel H.G. (2015) Mineralogy, nucleation and growth of dolomite in the laboratory and sedimentary environment: A review. *Sedimentology*, **62**, 1749-1769.

Gysi A.P. and Stefánsson A. (2008) Numerical modelling of CO_2-water-basalt interaction. *Mineralogical Magazine*, **72**, 55-59.

Gysi A.P. and Stefánsson A. (2012) CO_2-water-basalt interaction. Low temperature experiments and implications for CO_2 sequestration into basalts. *Geochimica et Cosmochimica Acta*, **81**, 129-152.

Hardie L.A. (1996) Secular variation in seawater chemistry: An explanation for the coupled secular variation in the mineralogies of marine limestones and potash evaporates over the past 600 m.y. *Geology*, **24**, 279-283.

Helgeson H.C. (1969) Thermodynamics of hydrothermal systems at elevated temperatures and pressures. *American Journal of Science*, **267**, 729-804.

Higgins S.R. and Hu X. (2005) Self-limiting growth on dolomite: Experimental observations with in situ atomic force microscopy. *Geochimica et Cosmochimica Acta*, **69**, 2085-2094.

Higgins S.R., Eggleston C.M., Knauss K.G. and Boro C.O. (1998) A hydrothermal atomic force microscope for imaging in aqueous solution up to 150 °C. *Review of Scientific Instruments*, **69**, 2994-2998.

Holland H.D. (2005) Sea level, sediments, and the composition of seawater. *American Journal of Science*, **305**, 220-239.

Hu X., Grossie D.A. and Higgins S.R. (2005) Growth and dissolution kinetics at the dolomite-water interface: An in-situ scanning probe microscopy study. *American Mineralogist*, **90**, 963-968.

Hu X., Joshi P., Mukhopadhyay S. M. and Higgins S. R. (2006). X-ray photoelectron spectroscopic studies of dolomite surfaces exposed to undersaturated and supersaturated

aqueous solutions. *Geochim. Cosmochim. Acta* **70**, 3342-3350.

Johnson J.W., Oelkers E.H. and Helgeson H.C. (1992) SUPCRT92: A software package for calculating the standard molal properties of minerals gases, aqueous species and reactions among them from 1 to 5000 bars and 0 to 1000 °C. *Computers & Geosciences,* **18**, 899-947.

Jordan G. and Astilleros J.M. (2006) In situ HAFM study of the thermal dehydration on gypsum (010) surfaces. *American Mineralogist*, **91**, 619-627.

Jordan G., Higgins S.R., Eggleston C.M., Swapp S.M., Janney D.E., and Knauss K.G. (1999) Acidic dissolution of plagioclase: in-situ observations by hydrothermal atomic force microscopy. *Geochim. Cosmochim. Acta* **63**, 3183-3191.

Kaczmarek S. and Sibley D. (2007). A comparison of nanometer-scale growth and dissolution features on natural and synthetic dolomite crystals: Implications for the origin of dolomite. *J. Sediment. Res.* **77**, 424-432.

Kaczmarek S.E. and Sibley D.F. (2014) Direct physical evidence of dolomite recrystalliza-tion. *Sedimentology*, **61**, 1862-1882.

Kaszuba J.P., Navarre-Sitchler A., Thyne G., Chopping C. and Meuzelaar T. (2011) Supercritical carbon-dioxide and sulfur in the Madison Limestone: A natural analog in southwest Wyoming for geologic carbon-sulfur co-sequestration. *Earth & Planetary Science Letters*, **309**, 131-140.

Katz A. and Matthews A. (1977). The dolomitization of CaCO3: an experimental study at 252-295 °C. *Geochim. Et Cosmochim. Acta 41*, 297-304.

Kessels L.A., Sibley D.F. and Nordeng S.H. (2000) Nanotopography of synthetic and natural dolomite crystals. *Sedimentology*, **47**, 173-186.

Land L.S. (1998) Failure to precipitate dolomite at 25 °C from dilute solution despite 1000-fold oversaturation after 32 years. *Aquatic Geochemistry*, **4**, 361-368.

Lippmann F. (1973) *Sedimentary carbonate minerals*. Springer-Verlag, New York, 228 pp.

Lowenstein T.K., Timofeeff M.N., Brennan S.T., Hardie L.A. and Demicco R.V. (2001) Oscillations in Phanerozoic seawater chemistry: Evidence from fluid inclusions. *Science*, **294**, 1086-1088.

Matter, J.M., Stute, M., Snaebjornsdottir, S.O., Oelkers, E.H., Gislason, S.R., Arandottir, E.S., Sigfusson, B., Gunnarsson, I., Sigurdardottir, H., Gunnlaugsson, E., Axelsson, G., Alfredsson, H., Wolff-Beonisch, D., Mesfin, K., Taya, D., Hall, J., Dideriksen, K., and Broecker, W. S. (2016) Rapid carbon mineralization for permanent disposal of anthroprogenic carbon dioxide emissions. *Science,* **352,** 1312-1314.

Mackenzie F.T. and Andersson A.J. (2013) The marine carbon system and ocean acidification during Phanerozoic time. *Geochemical Perspectives*, **2**, 1-227.

Mackenzie F.T. and Morse J.W. (1992) Sedimentary carbonates through Phanerozoic time. *Geochimica et Cosmochimica Acta*, **56**, 3281-3295.

Millero F., Huang F., Graham T. and Pierrot D. (2007) The dissociation of carbonic acid in

NaCl solutions as a function of concentration and temperature. *Geochimica et Cosmochimica Acta*, **71**, 46-55.

Montes-Hernandez G., Findling N., Renard F. and Auzende A.-L. (2014) Precipitation of ordered dolomite via simultaneous dissolution of calcite and magnesite: New experimental insights into an old precipitation enigma. *Crystal Growth & Design*, **14**, 671-677.

Moore J., Adams M., Allis R., Lutz S. and Rauzi. S. (2005) Mineralogical and geochemical consequences of the long term presence of CO_2 in natural reservoirs: An example of the Springerville-St. Johns Field, Arizona and New Mexico. *Chemical Geology,* **201**, 365-385.

Moreira N.F., Walter L.M., Vasconcelos C., McKenzie J.A. and McCall P.J. (2004) Role of sulfide oxidation in dolomitization: sediment and pore-water geochemistry of a modern hypersaline lagoon system. *Geology*, **32**, 701-704.

Oelkers E.H., Gislason S.R. and Matter J. (2008) Mineral carbonation of CO_2. *Elements*, **4**, 333-337.

Parkhurst D.L. and Appelo C.A.J. (1999) *User's guide to PHREEQC (version 2) - A computer program for speciation, batch-reaction, one-dimensional transport, and inverse geochemical calculations*. United States Geological Survey Water-resources Investigation Report 99-4259, 312 pp.

Roberts J. A., Kenward P.A., Fowle D.A., Goldstein R.H., González L.A., and Moore D.S. (2013) Surface chemistry allows for abiotic precipitation of dolomite at low temperature. *Proc. Natl. Acad. Sci. USA* **110**, 14540-14545.

Rodriguez-Blanco J.D., Shaw S. and Benning L.G. (2015) A route for direct crystallization of dolomite. *American Mineralogist*, **100**, 1172-1181.

Saldi G.D., Jordan G., Schott J. and Oelkers E.H. (2009) Magnesite growth rates as a function of temperature and saturation state. *Geochimica et Cosmochimica Acta*, **73**, 5646-5657.

Saldi G.D., Schott J., Pokrovsky O.S., Gautier Q. and Oelkers E.H. (2012) An experimental study of magnesite precipitation rates at neutral to alkaline conditions and 100-200 °C as a function of pH, aqueous solution composition and chemical affinity. *Geochimica et Cosmochimica Acta*, **83**, 93-109.

Sánchez-Román M., Vasconcelos C., Schmid T., Dittrich M., McKenzie J.A., Zenobi R. and Rivadeneyra M.A. (2008) Aerobic microbial dolomite at the nanometer scale: Implications for the geologic record. *Geology*, **36**, 879-882.

Stanley S.M. and Hardie L.A. (1999) Hypercalcification: Paleontology links plate tectonics and geochemistry to sedimentology. *GSA Today*, **9**, 2-7.

Tribble J.S., Arvidson R.S., Lane M. and Mackenzie F.T. (1995) Crystal chemistry, and thermodynamic and kinetic properties of calcite, dolomite, apatite, and biogenic silica: Applications to petrographic problems. *Sedimentary Geology*, **95**, 11-51.

Tutolo B.M., Luhman A.J., Kong X.-Z., Saar M.O. and Seyfried W.E. (2014) Experimental observation of permeability changes in dolomite at CO_2 sequestration conditions. *Environmental Science & Technology*, **48**, 2445-2452.

van Lith Y., Warthmann R., Vasconcelos C. and McKenzie J.A. (2003) Sulphate-reducing

bacteria induce low-temperature Ca-dolomite and high Mg-calcite formation. *Geobiology*, **1**, 71-79.

Vasconcelos C. and McKenzie J.A. (1997) Microbial mediation of modern dolomite precipitation and diagenesis under anoxic conditions, Lagoa Vermelha, Rio de Janeiro, Brazil. *Journal of Sedimentary Research,* **67**, 378-390.

Vasconcelos C., McKenzie J.A., Bernasconi S., Grujic D. and Tien A.J. (1995) Microbial mediation as a possible mechanism for natural dolomite formation at low temperatures. *Nature*, **377**, 220-222.

Wang X.Y., Alvarado V., Swoboda-Colberg N. and Kazszuba J.P. (2013) Reactivity of dolomite in water-saturated supercritical carbon-dioxide: Significance for carbon capture and storage and for enhanced oil and gas recovery. *Energy Conversion & Management*, **65**, 564-573.

Warren J. (2000) Dolomite: Occurrence, evolution and economically important associations. *Earth Science Reviews*, **52**, 1-81.

Warthmann R., van Lith Y., Vasconcelos C., McKenzie J.A. and Karpoff A.M. (2000) Bacterially induced dolomite precipitation in anoxic culture experiments. *Geology*, **28**, 1091-1094.

Wright D.T. and Wacey D. (2005) Precipitation of dolomite using sulphate-reducing bacteria from the Coorong Region, South Australia: Significance and implications. *Sedimentology*, **28**, 987-1008.

Xu M., Sullivan K., VanNess G., Knauss K.G., and Higgins S.R. (2013) Dissolution kinetics and mechanisms at dolomite-water interfaces: effects of electrolyte specific ionic strength. *Environ. Sci. Technol.* **47**, 110-118.

Xu T.F., Apps J.A. and Pruess K. (2003) Reactive geochemical transport simulation to study mineral trapping for CO_2 disposal in deep arenaceous formation. *Journal of Geophysical Research-Solid Earth*, **108**, 2071.

Figure Captions

Figure 1: HAFM deflection image showing the development of etch pits after the first 3 minutes of dissolution at 100 °C (From experiment Sunk-19).

Figure 2: Sequence of HAFM deflection images showing the formation and spreading of etch-pits on the (104) surface of dolomite at 80 °C during experiment Eugui-09 at pH = 8.14.

Figure 3: HAFM deflection images showing an inert (104) dolomite surface during growth experiment Sunk-48-A (T= 40 °C; Ω_{Dol}= 2.9). The left image (A) was recorded more than 1 h and the right image more than 2 h 20 min after the start of the experiment; during this time the surface showed no morphological change; the large cleavage step (white/rose diagonal feature) can serve as reference. Note that the scanning area is drifting to the upper right due to piezo creep.

Figure 4: The development of a single layer template growth on a (104) surface of dolomite as recorded by HAFM deflection images (Sunk-09). Precipitation starts on a surface which had been pre-cleaned in-situ via dissolution in MQ-water at 100 °C and monitored by HAFM (A). Pre-dissolution of some dolomite layers stopped just after developing a small etch pit in the lower left area of image A. As precipitation begins the surface is rapidly covered by a ~ 3 Å thick layer (B and C) which expands in obtuse step directions. Note steps are not propagating perpendicular to the initial step front but are rather curving forward (B) and do not close the small etch pit (which is atypical for layer-wise growth of carbonates) but grow around it (C). The precipitation apparently stopped after the formation of one layer of carbonate was complet and the initial surface was reproduced (D).

Figure 5: Growth of monolayer steps on a dolomite cleavage surface at 80 °C (Ω_{Dol} = 479, Eugui-10) after an initial period of dissolution at pH 4.0 and ambient temperature. Three layers were observed to grow during the experiment inside the main etch pit. After that the first layer was completed (a, b), the growth of the second layer (c) proceeded slower while the advancing steps developed a rough morphology and irregular shape.

Figure 6: Growth of single carbonate layers on dolomite (104) surface during experiment Eugui-11A, at 90 °C and Ω_{Dol} = 933 (a) and experiment 11B at 100 °C and Ω_{Dol} = 1513 (b). The growth of pre-existing layer was accompanied and followed by the 2D-nucleation of rounded growth-islands at both experimental conditions. The black arrows indicate the growth direction of pre-existing steps and the main growth orientation of nucleated layers advancing in the acute step direction.

Figure 7: Sequence of HAFM defelction images illustrating the irregular growth of carbonate monolayers at the dolomite (104) cleavage surface at 100 °C during experiment Eugui-12.

Table 1:   Electron microprobe analyses of both dolomite single crystals used in this study.

	Eugui (single xtl)	Sunk (single xtl)
CaO	29.89	29.18
MgO	20.89	20.39
FeO	0.5568	0.9701
MnO	0.0807	0.1613
ZnO	0.0387	0.0346
CuO	0.0183	0.0238
calc. CO_2	48.53	49.24
measured points	94	98
chem. formula based on six oxygens	$Ca_{1.005}Mg_{0.977}Fe_{0.015}Mn_{0.002}Zn_{0.001}(CO_3)_2$	$Ca_{0.998}Mg_{0.971}Fe_{0.026}Mn_{0.004}Zn_{0.001}(CO_3)_2$

Table 2: Summary of inlet solution compositions for hydrothermal atomic force microscopy (HAFM) experiments on dolomite.

Experiment	pH	$c_{CaCl2*2H2O}$ (mmol/kg)	$c_{MgCl2*6H20}$ (mmol/kg)	Alkalinity (mmol/kg)	NaCl (g/kg)	1N HCl (mL/L)	NaOH 0.1 M (mL/L)	CO_2 saturation (1 bar)
Eugui-01	6.59	0.606	57.4	45.9	0.2003	15.6	-	-
Eugui-02	6.32	0.535	48.5	30.0	0.0266	19.8	-	-
Eugui-03-A	6.59	0.286	54.9	45.9	0.1895	15.8	-	-
Eugui-03-B	6.59	0.286	54.9	45.9	0.1895	15.8	-	-
Eugui-04	7.86	0.501	0.502	0.986	5.6678	-	-	-
Eugui-06	7.86	0.590	0.555	0.987	5.6678	-	-	-
Eugui-08	8.30	0.0092	0.0101	100	0.0529	-	-	-
Egui-09	9.45	0.180	0	n.d.	5.844	-	0.44	-
Eugui-10	8.21	0.040	0.344	22.14	5.844	-	-	-
Eugui-11A	8.18	0.052	0.3397	22.75	5.844	-	-	-
Eugui-11B	8.18	0.052	0.3397	22.75	5.844	-	-	-
Eugui-12	8.16	0.027	0.3237	21.14	5.844	-	-	-
Sunk-01	6.53	4.68	5.21	1.98	4.0930	1.0	-	-
Sunk-02	6.43	10.4	16.0	1.63	0.8780	1.0	-	-
Sunk-03	6.13	8.20	10.4	1.49	1.9971	1.8	-	-
Sunk-04	5.95	9.73	12.3	1.57	1.2623	2.9	-	-
Sunk-05	6.15	8.29	10.5	1.57	1.9961	1.8	-	-
Sunk-06	6.12	9.52	12.2	1.58	1.3162	2.0	-	-
Sunk-07	6.10	6.34	24.6	2.60	0.2765	3.3	-	-
Sunk-08	6.15	24.2	6.06	0.763	0.4171	0.9	-	-
Sunk-09	6.19	5.94	25.3	2.17	0.3379	2.2	-	-
Sunk-10	6.18	24.4	6.02	0.947	0.4092	1.0	-	-
Sunk-11	5.67	50.0	50.5	2.01	-	5.0	-	-
Sunk-12	6.23	0.323	38.3	10.1	0.4198	8.8	-	-
Sunk-13	6.19	0.509	24.5	7.05	0.5052	7.4	-	-
Sunk-14	6.36	0.117	26.8	10.1	0.5236	7.0	-	-
Sunk-15	6.16	0.122	26.7	10.1	0.2828	11.2	-	-
Sunk-16	6.30	0.495	27.1	11.1	0.4212	8.8	-	-
Sunk-17	6.18	0.643	25.2	7.73	0.4559	8.2	-	-
Sunk-18	8.45	0.0088	0.0058	52.4	0.0445	-	-	-
Sunk-19	4.84	10.6	10.1	1.62	0.0952	38.4	-	-
Sunk-21	8.36	0.0198	0.102	5.59	-	-	-	-
Sunk-23	6.23	1.03	12.4	7.52	-	8.0	-	-
Sunk-24	5.51	48.5	56.9	9.99	-	-	-	saturated
Sunk-25	5.71	48.1	55.5	9.98	-	-	-	saturated
Sunk-26	5.77	52.4	58.0	4.98	-	-	-	saturated
Sunk-27	5.57	50.7	56.2	4.99	-	-	-	saturated
Sunk-28	5.66	49.4	55.9	7.49	-	-	-	saturated

Table 2: Continued

Experiment	pH	$c_{CaCl2 \cdot 2H2O}$ (mmol/kg)	$c_{MgCl2 \cdot 6H2O}$ (mmol/kg)	Alkalinity (mmol/kg)	NaCl (g/kg)	1N HCl (mL/L)	NaOH 0.1 M (mL/L)	CO_2 saturation (1 bar)
Sunk-31	7.10	0.178	34.0	2.71	-	0.3	-	-
Sunk-32	6.39	105	112	2.62	-	0.9	-	-
Sunk-33	6.42	10.6	10.1	1.32	-	0.9	-	-
Sunk-34	6.71	10.6	10.3	1.64	0.0265	0.5	-	-
Sunk-35	6.39	57.6	61.3	1.97	-	0.9	-	-
Sunk-36	6.41	0.0055	32.2	1.86	0.0209	1.1	-	-
Sunk-38	6.41	32.8	0.0010	1.86	0.0209	1.1	-	-
Sunk-39	6.55	32.4	0.0093	2.08	0.0337	0.9	-	-
Sunk-40	6.41	16.4	16.1	1.86	0.0209	1.1	-	-
Sunk-41	3.93	10.7	1.12	0.0048	-	30.0	-	-
Sunk-42	6.28	5.78	1.10	15.3	0.3113	14.7	-	-
Sunk-43	5.79	8.22	1.11	7.68	0.1108	22.3	-	-
Sunk-44	5.58	0.0071	51.8	10.0	-	-	-	saturated
Sunk-45	5.58	0.0099	51.8	10.0	-	-	-	saturated
Sunk-46	5.59	48.6	0.0022	10.1	-	-	-	saturated
Sunk-47	5.60	47.9	0.0044	10.1	-	-	-	saturated
Sunk-48-A	5.59	19.2	31.1	10.0	-	-	-	saturated
Sunk-48-B	5.59	19.2	31.1	10.0	-	-	-	saturated
Sunk-49-A	5.59	17.6	29.4	10.1	-	-	-	saturated
Sunk-49-B	5.59	17.6	29.4	10.1	-	-	-	saturated
Sunk-50-A	5.38	22.1	27.0	6.24	-	-	-	saturated
Sunk-50-B	5.38	22.1	27.0	6.22	-	-	-	saturated
Sunk-51	7.08	0.0435	7.35	5.23	0.5370	0.8	-	-
Sunk-52	7.02	4.91	0.0007	0.796	0.5757	0.1	-	-
Sunk-53	6.76	10.8	0.0276	2.66	0.5350	0.8	-	-
Sunk-54	6.94	5.43	3.69	3.95	0.5360	0.8	-	-
Sunk-55	4.12	0.0137	521	0.673	-	-	-	saturated
Sunk-56	4.94	5.42	260	1.67	0.2922	5.0	-	saturated
Sunk-57	6.38	2.81	30.3	7.65	-	5.0	-	-
Sunk-59-A	6.38	1.08	32.5	7.71	-	5.0	-	-
Sunk-59-B	6.38	1.08	32.5	7.71	-	5.0	-	-
Sunk-61	6.38	1.93	29.8	7.68	-	5.0	-	-

Table 3: Summary of the results of hydrothermal atomic force microscopy (HAFM) experiments on dolomite (104) surfaces.

Experiment	Temp (°C)	pH_{calc}	Ionic strength	Ω_{Dol}	a_{Ca+2} (x 10^{-4})	a_{Mg+2} (x 10^{-4})	a_{CO3-2} (x 10^{-7})	Observation
Eugui-01	40	6.50	0.217	220	1.65	176	48.6	1 layer
Eugui-02	40	6.23	0.183	26.4	1.60	162	17.9	1 layer
Eugui-03-A	40	6.50	0.209	103	0.787	170	49.2	1 layer
Eugui-03-B	60	6.47	0.207	336	0.746	161	54.5	1 layer
Eugui-04	100	7.50	0.099	10.7	1.71	1.86	16.3	no reaction
Eugui-06	100	7.49	0.100	13.6	2.01	2.05	16.1	no reaction
Eugui-08	100	8.10	0.101	49.6	0.0064	0.014	6667	1 layer
Eugui-09	80	8.14	0.099	<< 1	0.651	0.005	4.40	dissolution
Eugui-10	80	7.99	0.100	467.7	0.098	1.079	1242	3 layers
Eugui-11A	90	7.96	0.100	933.3	0.1171	1.011	1220	multi-layer
Eugui-11B	100	7.95	0.100	1513.6	0.1062	0.954	1218	multi-layer
Eugui-12	100	7.94	0.099	660.7	0.057	0.928	1102	multi-layer
Sunk-01	100	6.51	0.101	41.6	15.9	19.3	3.26	1 layer*
Sunk-02	100	6.37	0.095	80.6	36.3	61.2	1.69	1 layer*
Sunk-03	100	6.09	0.091	11.5	28.9	40.1	0.883	1 layer
Sunk-04	100	5.91	0.090	7.4	34.5	47.5	0.594	1 layer
Sunk-05	100	6.11	0.092	14.3	29.1	40.4	0.976	1 layer
Sunk-06	100	6.08	0.089	15.7	33.8	47.1	0.880	1 layer
Sunk-07	100	6.04	0.100	38.5	21.6	92.1	1.23	1 layer
Sunk-08	100	6.09	0.098	4.2	84.1	23.1	0.410	no reaction
Sunk-09	100	6.13	0.101	38.4	20.3	94.7	1.25	1 layer
Sunk-10	100	6.12	0.099	7.3	84.5	22.9	0.544	1 layer
Sunk-11	100	5.57	0.297	11.1	121	142	0.224	1 layer
Sunk-12	100	6.17	0.133	57.3	0.962	126	6.07	3 layers*
Sunk-13	100	6.14	0.093	39.3	1.72	89.9	4.47	3 layers*
Sunk-14	100	6.31	0.101	39.4	0.377	94.4	9.31	5 layers*
Sunk-15	100	6.11	0.100	16.6	0.394	94.1	5.92	3 layers*
Sunk-16	100	6.25	0.103	148	1.58	94.3	8.84	1 layer*
Sunk-17	100	6.13	0.096	56.2	2.14	91.5	4.75	2 layers*
Sunk-18	100	8.21	0.053	28.1	0.0086	0.011	4783	no reaction
Sunk-19	100	4.81	0.102	0.0	36.2	37.7	0.050	dissolution
Sunk-21	100	8.01	0.006	103	0.094	0.586	383	1 layer
Sunk-23	40	6.14	0.054	1.7	4.59	58.8	4.49	dissolution
Sunk-24	100	5.40	0.307	129	113	154	0.762	3 layers*
Sunk-25	100	5.61	0.302	324	113	151	1.22	3 layers*
Sunk-26	100	5.66	0.320	111	123	158	0.669	1 layer*
Sunk-27	100	5.46	0.310	44.1	120	155	0.432	1 layer*
Sunk-28	100	5.55	0.306	146	116	153	0.802	1 layer*
Sunk-29	100	6.94	0.102	157	1.09	126	9.46	1 layer

Table 3. Continued

Experiment	Temp	pH$_{calc}$	Ionic strength	Ω_{Dol}	a$_{Ca+2}$	a$_{Mg+2}$	a$_{CO3-2}$	Observation
Sunk-31	100	6.91	0.102	76.7	0.601	127	8.89	1 layer
Sunk-32	100	6.22	0.614	575	203	262	0.920	1 layer*
Sunk-33	100	6.36	0.063	47.6	41.8	43.1	1.44	1 layer*
Sunk-34	100	6.63	0.064	243	41.7	43.6	3.24	1 layer*
Sunk-35	100	6.25	0.344	261	133	166	0.962	1 layer*
Sunk-36	100	6.33	0.097	0.1	0.019	122	1.69	dissolution
Sunk-38	100	6.34	0.100	0.0	112	0.0038	1.72	dissolution
Sunk-39	100	6.46	0.099	0.3	111	0.035	2.57	dissolution
Sunk-40	100	6.33	0.098	128	56.5	60.8	1.71	2 layers*
Sunk-41	100	3.93	0.065	0.0	42.2	4.75	0.00066	dissolution
Sunk-42	100	6.27	0.054	287	20.9	4.25	15.9	1 layer
Sunk-43	100	5.78	0.058	11.1	31.4	4.52	2.48	1 layer
Sunk-44	100	5.51	0.154	0.1	0.020	166	1.22	dissolution
Sunk-45	100	5.50	0.154	0.1	0.028	166	1.21	dissolution
Sunk-46	100	5.53	0.149	0.0	140	0.0071	1.36	dissolution
Sunk-47	100	5.53	0.147	0.0	139	0.014	1.37	dissolution
Sunk-48-A	40	5.49	0.155	2.9	63.9	116	1.11	no reaction
Sunk-48-B	70	5.46	0.154	17.3	59.9	109	1.24	1 layer
Sunk-49-A	40	5.50	0.145	2.8	59.8	111	1.14	no reaction
Sunk-49-B	70	5.47	0.144	16.7	56.1	104	1.29	1 layer
Sunk-50-A	50	5.27	0.149	0.8	74.1	101	0.46	dissolution
Sunk-50-B	100	5.31	0.147	18.3	65.6	89.6	0.494	1 layer*
Sunk-51	70	6.97	0.036	9.9	0.204	36.4	27.9	no reaction
Sunk-52	70	6.90	0.025	0.0	26.1	0.0039	3.76	dissolution
Sunk-53	70	6.64	0.045	0.5	49.4	0.134	6.49	dissolution
Sunk-54	70	6.82	0.040	171	25.1	18.1	14.8	1 layer
Sunk-55	120	4.01	1.275	0.0	0.020	874	0.0008	dissolution
Sunk-56	120	4.81	0.705	0.1	9.24	522	0.015	dissolution
Sunk-57	40	6.28	0.108	13.0	10.4	123	5.63	no reaction
Sunk-59-A	40	6.29	0.110	5.4	4.00	132	5.67	no reaction
Sunk-59-B	100	6.31	0.107	234	3.49	115	6.75	2 layers*
Sunk-61	40	6.29	0.104	9.3	7.21	122	5.76	no reaction

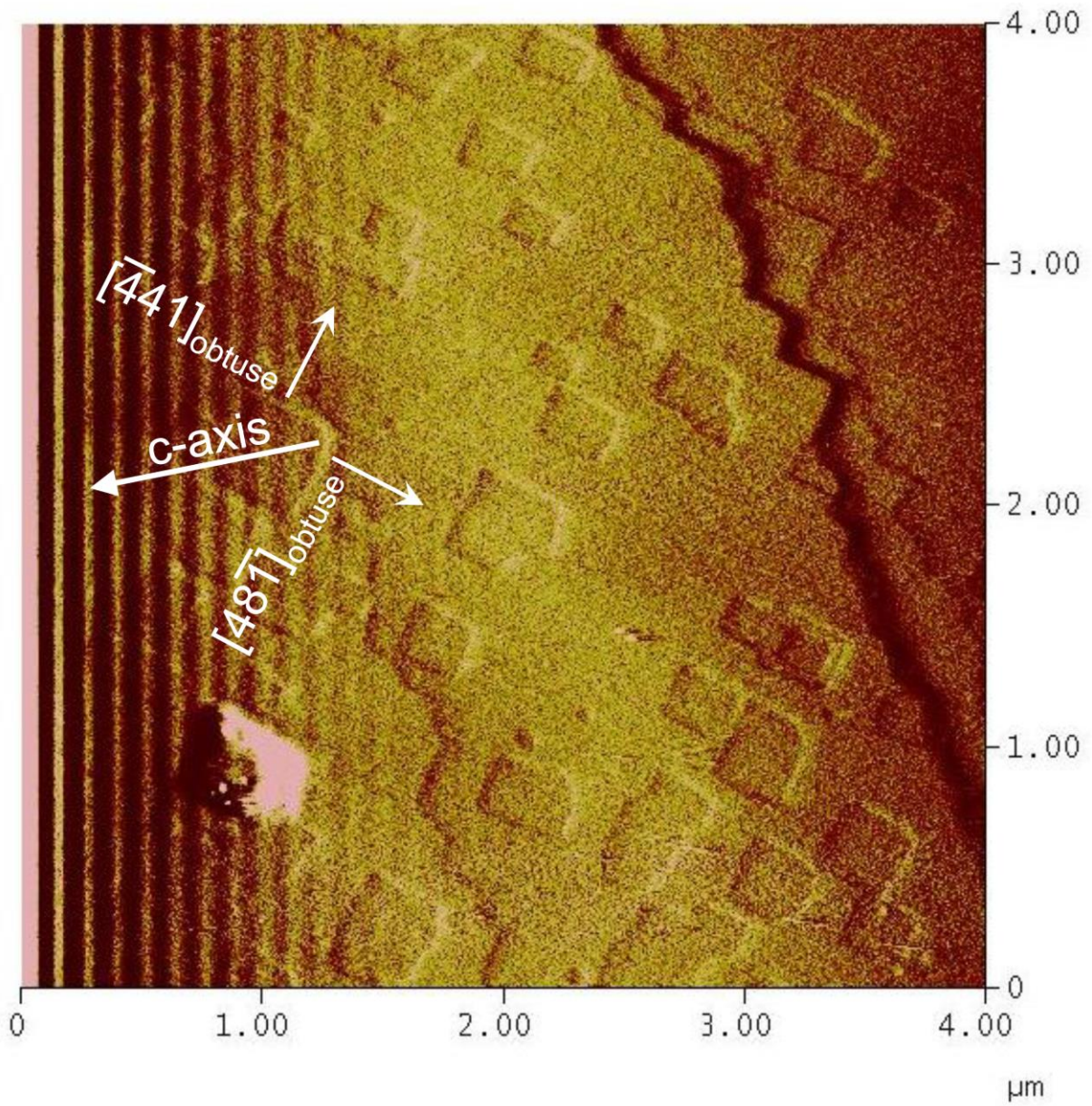* Growth seemed to continue but extremely slow.

Figure 1: HAFM deflection image showing the development of etch pits after the first 3 minutes of dissolution at 100 °C (From experiment Sunk-19).
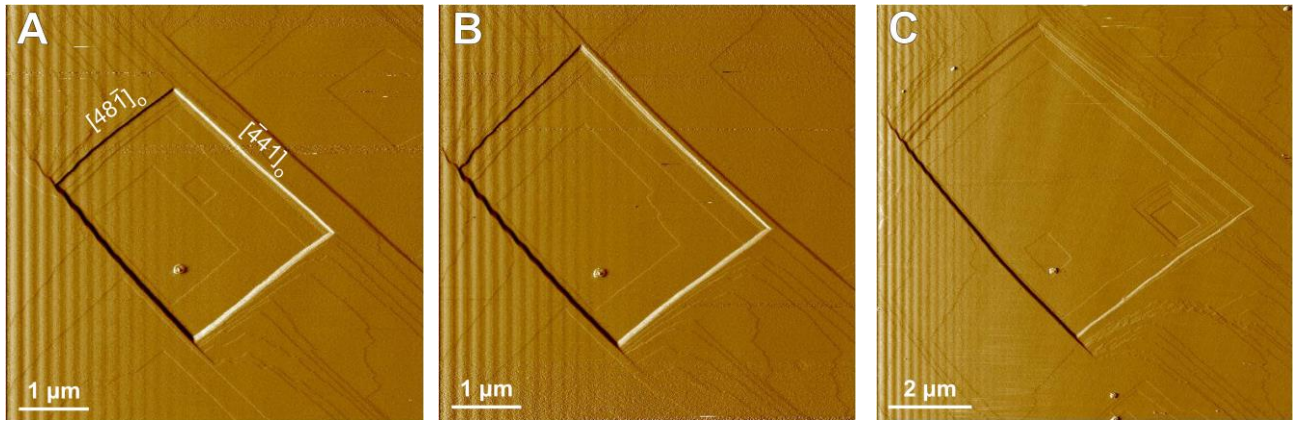
Figure 2: Sequence of HAFM deflection images showing the formation and spreading of etch-pits on the (104) surface of dolomite at 80 °C during experiment Eugui-09 at pH = 8.14.
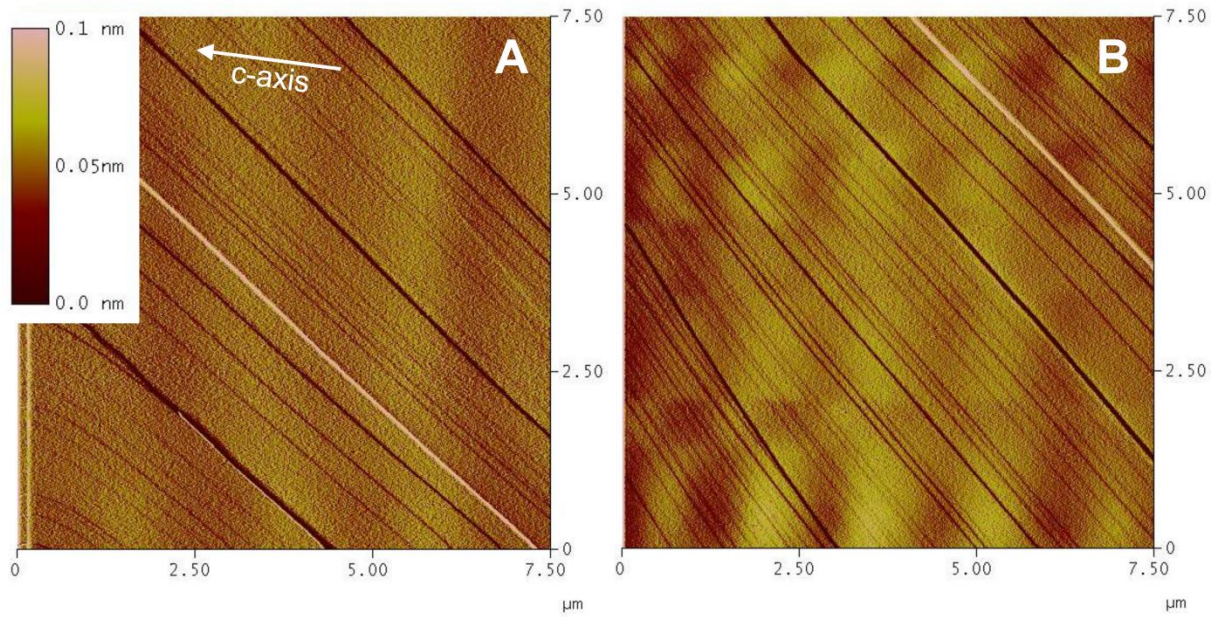
Figure 3: HAFM deflection images showing an inert (104) dolomite surface during growth experiment Sunk-48-A (T= 40 °C; Ω_{Dol}= 2.9). The left image (A) was recorded more than 1 h and the right image more than 2 h 20 min after the start of the experiment; during this time the surface showed no morphological change; the large cleavage step (white/rose diagonal feature) can serve as reference. Note that the scanning area is drifting to the upper right due to piezo creep.

Figure 4 The development of a single layer template growth on a (104) surface of dolomite as recorded by HAFM deflection images (Sunk-09). Precipitation starts on a surface which had been pre-cleaned in-situ via dissolution in MQ-water at 100 °C and monitored by HAFM (A). Pre-dissolution of some dolomite layers stopped just after developing a small etch pit in the lower left area of image A. As precipitation begins the surface is rapidly covered by a ~ 3 Å thick layer (B and C) which expands in obtuse step directions. Note steps are not propagating perpendicular to the initial step front but are rather curving forward (B) and do not close the small etch pit (which is atypical for layer-wise growth of carbonates) but grow around it (C). The precipitation apparently stopped after the formation of one layer of carbonate was complet and the initial surface was reproduced (D).
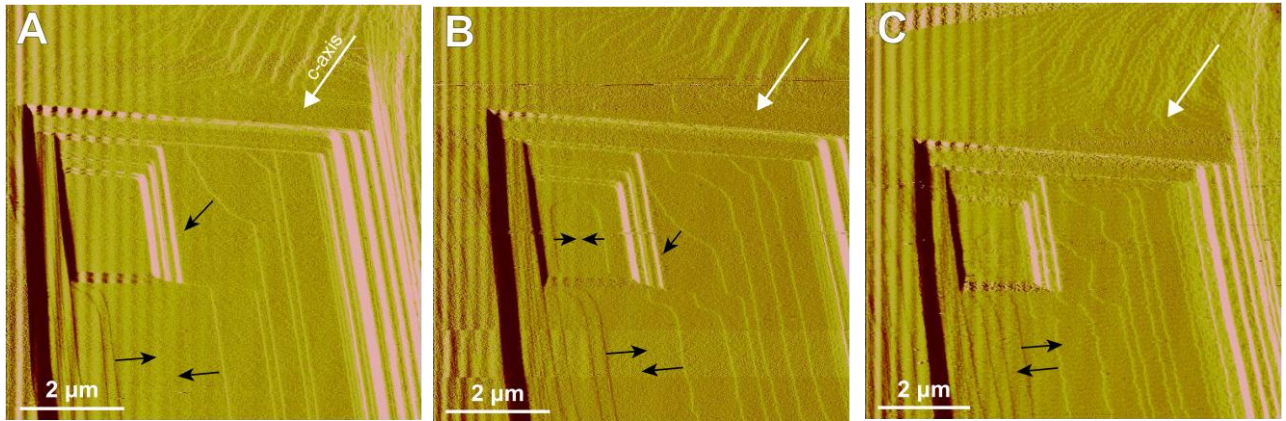
Figure 5 Growth of monolayer steps on a dolomite cleavage surface at 80 °C (Ω_{Dol} = 479, Eugui-10) after an initial period of dissolution at pH 4.0 and ambient temperature. Three layers were observed to grow during the experiment inside the main etch pit. After that the first layer was completed (a, b), the growth of the second layer (c) proceeded slower while the advancing steps developed a rough morphology and irregular shape.
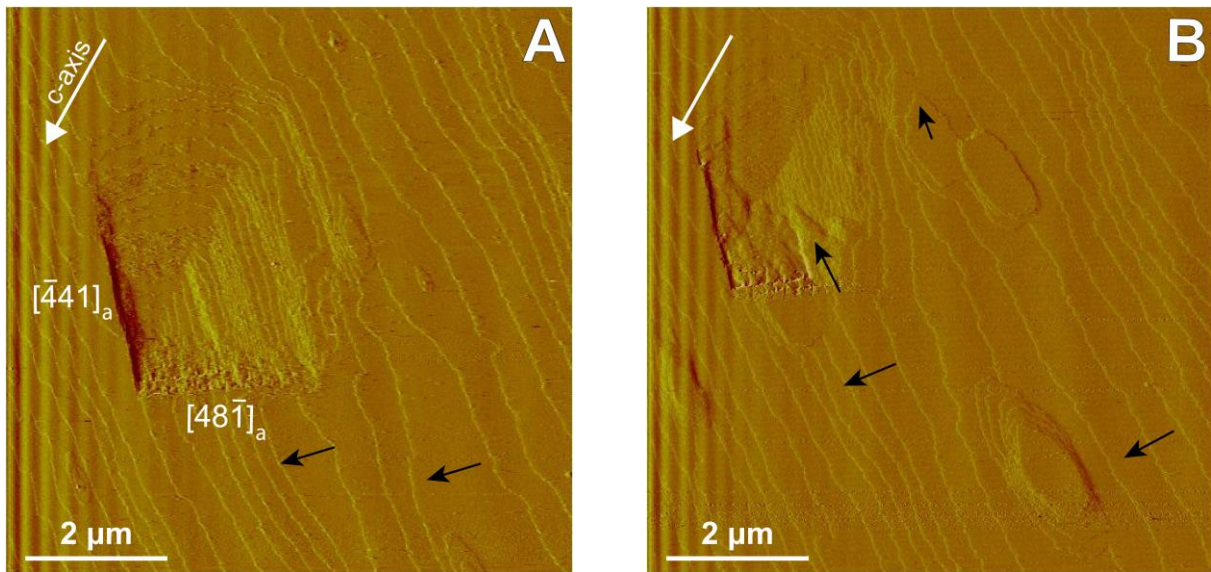
Figure 6 Growth of single carbonate layers on dolomite (104) surface during experiment Eugui-11A, at 90 °C and Ω_{Dol} = 933 (a) and experiment 11B at 100 °C and Ω_{Dol} = 1513 (b). The growth of pre-existing layer was accompanied and followed by the 2D-nucleation of rounded growth-islands at both experimental conditions. The black arrows indicate the growth direction of pre-existing steps and the main growth orientation of nucleated layers advancing in the acute step direction.
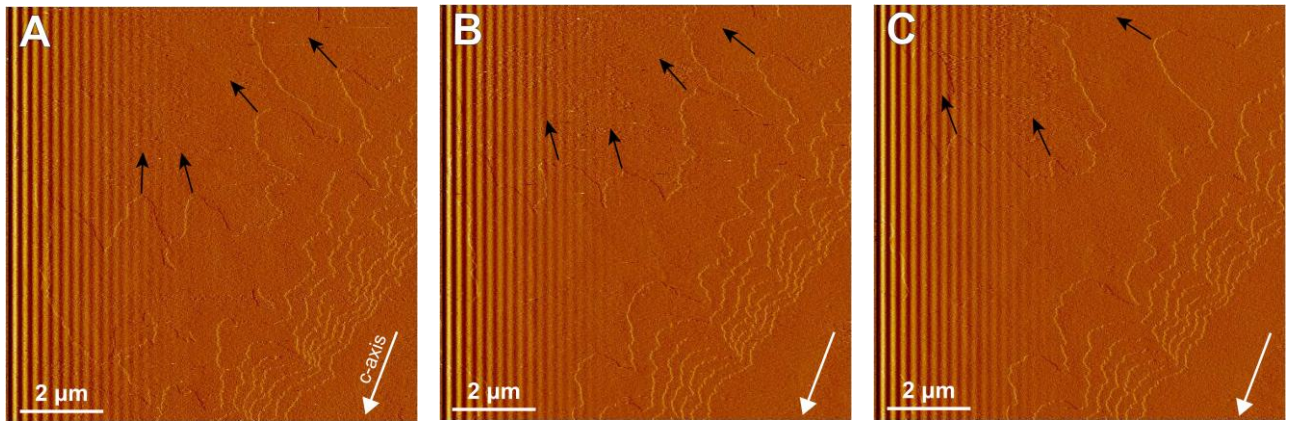
Figure 7 Sequence of HAFM defelction images illustrating the irregular growth of carbonate monolayers at the dolomite (104) cleavage surface at 100 °C during experiment Eugui-12.
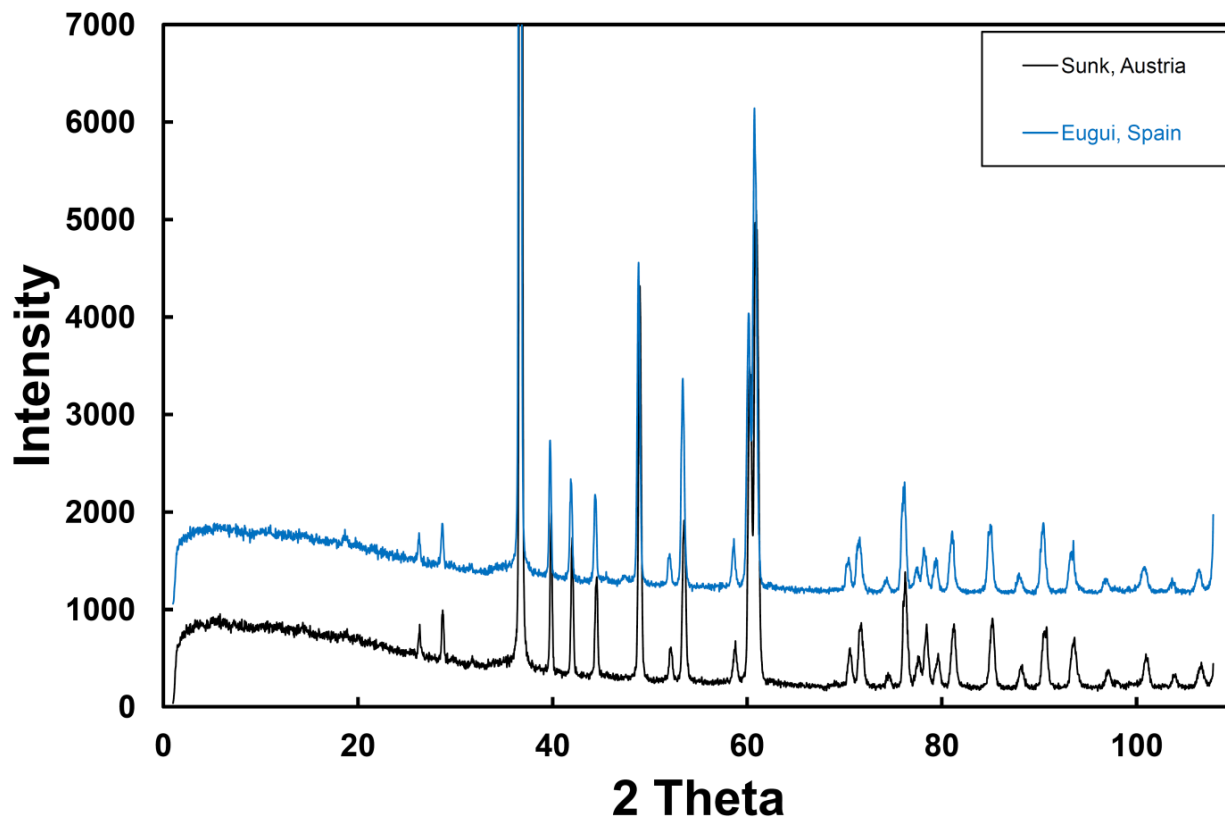
Electronic Supplement

Figure: Powder x-ray diffractogram of dolomite from Eugui, Spain, and Sunk, Austria.